Sensing Mechanism Elucidation of a Chemosensor Based on a Metal-Organic Framework (MOF) Selective to Explosive Aromatic Compounds

Yoan Hidalgo-Rosa[1], Manuel A. Treto-Suarez[1], Eduardo Schott[2], Ximena Zarate[1], and Dayan Paez-Hernandez[1]

[1]Universidad Andres Bello
[2]Pontificia Universidad Catolica de Chile

April 28, 2020

Abstract

Theoretical elucidation of the turn-off mechanism of the luminescence of a chemosensor based on a metal-organic framework (MOF) [Zn2(OBA)4(BYP)2] (BYP: 4,4'-bipyridine; H2OBA: 4,4'-oxybis(benzoic acid)), selective to nitrobenzene via quantum chemical computations is presented. The electronic structure and optical properties of Zn-MOF were investigated through the combination of density functional theory (DFT) and time-dependent-DFT methods. Our results indicate that the fluorescence emission is governed by a linker (BPY) to linker (OBA) charge transfer (LLCT) involving orbitals π-type. Next, interaction with the analyte was analyzed, where very interesting results were obtained, i.e. the LUMO is now composed by orbitals from nitrobenzene, which changes the emissive state of the Zn-MOF. This fact suggests that the LLCT process is blocked, inducing then the fluorescence quenching. Otherwise, the Morokuma-Ziegler energy decomposition and NOCV (Natural Orbitals for Chemical Valence) on the Zn-MOF-nitrobenzene interactions were studied in detail, which illustrate the possible channels of charge transfer between Zn-MOF and nitrobenzene. Finally, we believe that this proposed methodology can be applied to different chemosensor-analyte systems to evidence the molecular and electronic factors that govern the sensing mechanisms.

Keywords

Luminescence MOFs, TD-DFT, PET, Nitroaromatic compounds

Introduction

The interest on the chemical detection *in situ* of nitroaromatic compounds (NACs) accurately and reliably, is mainly associated with security, environment pollution, and human health. This fact has currently encouraged researches to focus on the design of new chemical sensors that show selective detection of NACs such as 2,4,6-trinitrophenol (TNP),[1] nitrobenzene (NB)[2], 2,6-dinitrotoluene (DNT)[3], among others.[4] Furthermore, these compounds are extensively used in many industrial processes and some of them are highly toxic or carcinogenic. Moreover, they are potent pollutants of soils and groundwaters.[5-6] On the other hand, a highlighted fact about these chemical compounds is that they represent a potential risk to security, due to their high explosive power as well as the easy access to them; being also used in the manufacture of improvised explosive devices.[7-8] In this sense, more research on their effective detection is needed as well as the implementation and improvement of devices used to this end. The performance principle of a chemical sensors is based on the change of an observable response upon interaction with analytes of interest. The observables are based on physical principles such as absorbance, transmittance, the polarization of light, luminescence, among others. In this context, Metal-Organic Frameworks (MOFs) have emerged as a very interesting alternative for the design of chemosensors due to their structural and photophysical features;

1

luminescence specifically.[9] MOFs are composed of metal centers or cluster-like arrangements called nodes connected by linkers, which are organic ligands.[10]This wide range of possibilities to get different structures of MOFs, with different nodes and linkers, confers to these materials different photophysical responses including luminescent properties.[11] In this regard, light emission can arise from either the ligand or the nodes, *i.e.* from the metal ions or metal clusters. The luminescence mechanism can involve energy transfer processes, ligand-to-ligand charge transfer (LLCT), ligand-to-metal charge transfer (LMCT) or metal-to-ligand charge transfer (MLCT) as well as metal-to-metal charge transfer (MMCT).[12] These inorganic and organic species confers them flexible coordination environment that leads to different secondary building units (SBUs) and then a variety of topologies of the network (*i.e.* IRMOF-n series based on the renowned MOF-5, the UiO series such as UiO-66, UiO-67, UiO-68, etc). [13-14] The importance of the porosity and the large surface area of MOFs is recognized as the system acts as a pre-concentrator of the targeted analyte, displaying host-guest interactions which can be modulated because of their synthetic versatility.[15-16] When the MOF encapsulates the analytes, the interactions that occur (host-guest) might induce changes in the photophysical properties, causing the activation or deactivation of the luminescent signal of the whole system.[17-18] This response to the emission intensity gives rise to an important classification that groups them as luminescent turn-off or turn-on chemosensor. In this sense, when the emission is very weakly or the system does not emit but the resulting luminescence is enhanced by adding the analyte, it is called a Turn-on chemosensor. While Turn-off chemosensors are systems whose luminescence is quenched after interaction with the chemical species of interest (Scheme 1). [19-20]
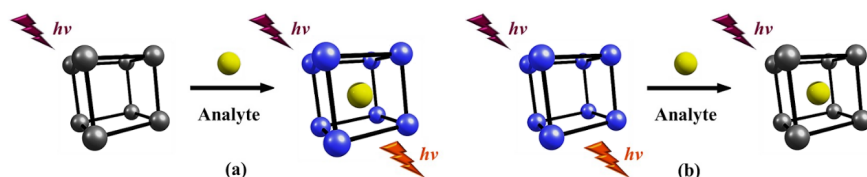

Scheme 1. Schematic representation of a chemosensor: (**a**) Turn-on of the luminescence, (b) Turn-off of the luminescence.

In this sense, luminescent chemical sensors based on MOFs have emerged as a successful alternative for sensing of NACs as they show intense luminescence, low limits of detection (LODs) (up to single-molecule level), specificity, tunable porosity, chemical functionality and the ability to use them as powdered materials directly without further treatments. Specifically, luminescent MOFs (LMOFs), based on d^{10} metal ions, have been of great interest for designing and synthesizing chemosensors selective to NACs. Regarding to this, Allendorf *et al.* in 2007 [21] pointed out the importance of the design of LMOFs based on closed-shell metal ions, and also taking into account that it is possible to tune the linker-centered emission by modifying the structure of the linker. This fact is mostly studied since this type of MOFs are unlikely metal light emisor, as the Zn-based and Cd-based LMOFs reported by W. Liu and co-workers.[22] Based on these premises, Lustig *et al.* (2016)[23] developed a series of LMOFs with ligand-centered emission. They performed the modification of the linkers (tetrakis(4-carboxyphenyl) ethylene) by both fluorination and elongation. Thus, the quantum yield of luminescence and thermal stability were improved in these systems, concluding that the adequate selection of the linker, whose emission can be increased or tuned, is a versatile strategy to design LMOFs based on closed-shell transition metal ions. In recent years, vast published literature has been reported about LMOFs in the area of chemical sensors selective to explosive aromatic compounds. In most cases, the most efficient reported mechanism of transduction, is through a luminescence quenching response (turn-off mechanism). This fact is due to the excellent electron-donating capability of MOFs, the strong electron-accepting ability of NACs and probability of photoinduced electron transfer (PET) between both systems.[24-25] In this mechanism, the detection pathway of the analyte involves a PET from the LMOFs to the guest deactivating the electronic emissive state. Here, the extinction of the luminescence requires an electron structure where the analyte orbitals have adequate energy to produce the PET. [26-27] Regarding

2

this, several studies of density functional theory (DFT) calculations have been reported, providing a more detailed description of the proposed sensing mechanism. From these results, researchers have proposed that the most probable PET mechanism is due to electron transfer from the conduction band (CB) of the MOF to lowest unoccupied molecular orbital (LUMO) of NACs.[24-28] Nevertheless, since most of the theoretical reports deal the computations of the MOF and analyte separately, which have limited the analysis to an orbital energy comparison between both structures, it becomes imperative to address the study of host-guest systems to design MOFs as sensors. This last is a remarkable topic recalled in literature due to their role in changes on the photophysical properties that govern the recognition mechanisms of analytes.[29-30] That is why we consider that MOF-analyte interaction study is a key to understand the path of the activation or deactivation of the luminescence in a sensing process in a more accurately protocol. The current status of computational methods and theoretical chemistry opens the possibility of investigating photo-physical processes that modulate the luminescent properties of LMOFs chemosensors. In this work, we investigated and assessed the turn-off fluorescence mechanism of the Zn-based LMOF [$Zn_2(OBA)_2(BYP)$]DMA, where H_2OBA: 4,4'-oxybis (benzoic acid); BYP: 4,4'-bipyridine; DMA = N, N'-dimethylacetamide, through quantum mechanics calculations, synthesized and reported by Jing Li *et al.* in 2011,[31] as a selective chemical sensor to high explosive NACs. A methodology including molecular and electronic properties of the systems, for evaluating the relationship between the structure of the LMOF and analyte-induced luminescence change was successfully established. In terms of MOF-analyte interaction, we are interested in the contribution of each term to the total interaction energy, *i.e* , electrostatic interaction, orbital interaction, a dispersive interaction as well as repulsive Pauli interaction. In this sense, it was demonstrated that the energy decomposition scheme proposed by Morokuma-Ziegler provides valuable information to this regard as well as NOCV (Natural Orbitals for Chemical Valence) calculations to characterize the charge transfer channels.[32-33]

Computational Details

According to Zhong-Min (2014)[34] and Lu (2019)[22] from the point of view of the molecular orbitals, MOFs can be treated as discrete molecular systems. This fact is especially applicable in LMOFs based on d^{10} metal, due that they present narrow band gaps energies and highly localized electronic states.[35] The LMOF understudy is formed by molecular units of [$Zn_2(OBA)_4$] (OBA=4,4'-oxybis (benzoic acid)) linked together forming two-dimensional (2D) networks where the ligand 4,4'-bipyridine (BYP) acts as linker between the [$Zn_2(OBA)_4$] units of two adjacent layers, to get a highly porous three-dimensional (3D) network. Therefore, in our system model, the structure was truncated to one node and six linkers [$Zn_2(OBA)_4(BYP)_2$], which we will refer to as Zn-MOF (see Figure 1). The truncated structural proposal has been previously used to describe the electronic structure, photophysical and catalytic properties in MOFs, where theoretical results have shown excellent agreement with the experimental data.[36] [37] [38][39]
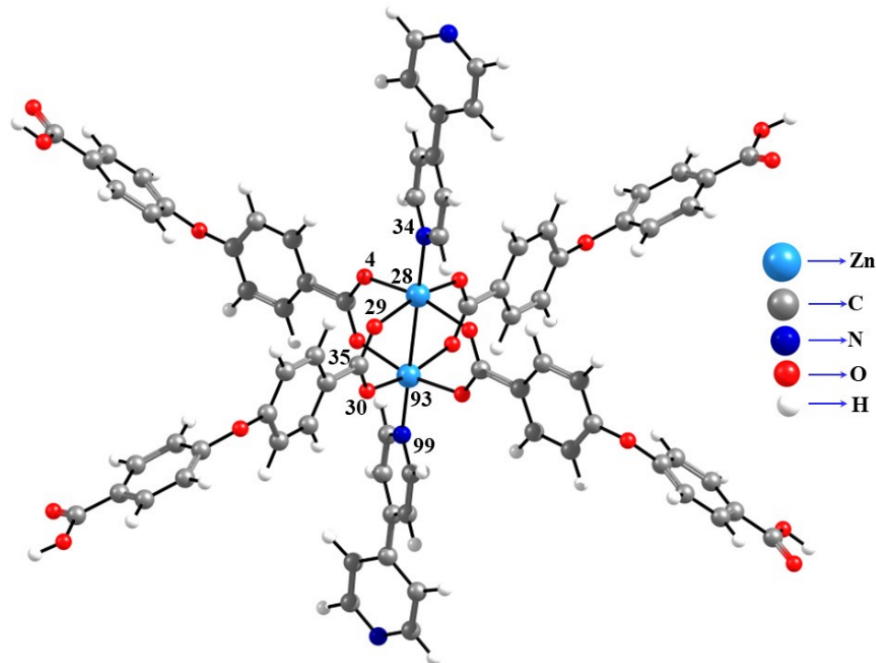
Figure 1. Optimized geometry of the truncated Zn-MOF (BP86/def2-TZVPP).

The first step consisted in optimizing the Zn-MOF as well as the interacting system Zn-MOF-analyte with the ORCA package.[40] All structures were optimized via the gradient-corrected Becke–Perdew (BP86)[41]exchange-correlation functional using the triple-zeta valence with two sets of polarization functions (def2-TZVPP) [42] basis set. In the second stage of this work, we performed a study of the optical properties of the Zn-MOF and Zn-MOF-analyte systems by means of the Time-dependent Density Functional Theory (TD-DFT) approach. To simulate the vertical transitions, 50 excitations were computed at the hybrid exchange-correlation functional (B3LYP) [43] as well as the Coulomb Attenuated Method (functional, CAM-B3LYP)[44] and def2-TZVPP basis set. Finally, we analyzed the nature of the interaction Zn-MOF-analyte based on the energy decomposition analysis (EDA) proposed by Morokuma–Ziegler.[45] The interaction energy (ΔE_{int}) between two defined fragments according to the EDA scheme can be divided into four components:

$$\Delta E_{int} = \Delta E_{Elec} + \Delta E_{Pauli} + \Delta E_{Orb} + \Delta E_{Disp} \quad (1)$$

Where ΔE_{Elec} accounts for the classical electrostatic interaction between the fragments as they are brought to their positions in the final structure. The second term ΔE_{Pauli} is related to the repulsive interaction of Pauli, between occupied orbitals of both molecular fragments. The third term ΔE_{Orb}expresses the possible interactions between molecular orbitals related to the charge transfer, polarization, etc. This term can be analyzed by the natural orbital of chemical valence method proposed by Mitoraj.[46-47] The term ΔE_{Disp}describes the dispersion forces acting between the fragments. We consider the long-range interactions, using Grimme's D3 dispersion correction for EDA calculations.[48]

Results and discussion

The geometrical parameters upon geometry optimization of the Zn-MOF are in good agreement with experimental X-ray data.[31] The results showed that the computed [Zn(28)–Zn(93)], [Zn(28)–N(34)] and [Zn(28)–O(29)] bond lengths are Å 2.84 Å, 2.08 Å, and 2.07 Å, while the experimental values for Zn-MOF are 2.89 Å 2.02 Å, and 2.04, respectively.[31] These are also consistent with theoretical reported 2.23 Å, 2.25 Å and 2.06 Å respectively values, computed at the PBE-D3/ Triple-zeta (TZP) theoretical level and used a truncated structural model, for this MOF by Ce Hao *et. al.* [24] in 2016.

Besides, the calculations reveal similar results regarding the [N(34)–Zn(28)–O(4)], and [O(29)–C(35)–O(30)] bond angles which are 97.8@and 123.5@, see the structure on Figure 1. These values agree with the experimental X-ray data which are 97.9@ and 124.2@ respectively[31] and reported 96.9@and 124.2@ theoretical values.[24].

These results suggest that the proposed structural truncated model is consistent with models previously reported and based on a fragmentation scheme. Based on this fact, the optical properties of the Zn-MOF were explored on the minimum optimized structure of the ground state (S_0) by means of TDDFT approaches. The simulated UV-vis spectrum using both CAM-B3LYP and B3LYP functional (with maxima of 248 and 281 nm respectively) showed an excellent agreement with the experimental absorption wavelength value[31], 280 nm. The TDDFT(B3LYP) computed values are closer to the experimental one, presumably due to the absence of the charge transfer between the metals and ligands. Table 1 reports the maximum absorption wavelength (in nanometer, nm), oscillator strengths (f) as well as the assignments to the electronic transitions with the largest f. The molecular orbitals involved in the excitations are localized along with the OBA linker as can be seen from Figure 2.

Table 1. Singlet - Singlet electronic transitions for Zn-MOF.

Zn-MOF	Funtional	λmax (nm)	f	Assignment	Active MO	Cts (%)
Absorption	B3LYP	281	1.31	$\pi(\Lambda^{OBA})$-$\pi^*(\Lambda^{OBA})$	H-2-L+2	43
				$\pi(\Lambda^{OBA})$-$\pi^*(\Lambda^{OBA})$	H-3-L+3	34
				$\pi(\Lambda^{OBA})$-$\pi^*(\Lambda^{OBA})$	H-L+3	14
	CAM-B3LYP	248	1.04	$\pi(\Lambda^{OBA})$-$\pi^*(\Lambda^{OBA})$	H-3-L+3	31
				$\pi(\Lambda^{OBA})$-$\pi^*(\Lambda^{OBA})$	H-2-L+2	28
				$\pi(\Lambda^{OBA})$-$\pi^*(\Lambda^{OBA})$	H-L+3	7

Where: H: is HOMO, L is LUMO, Cts (%) is contributions corresponding of electronic transitions.
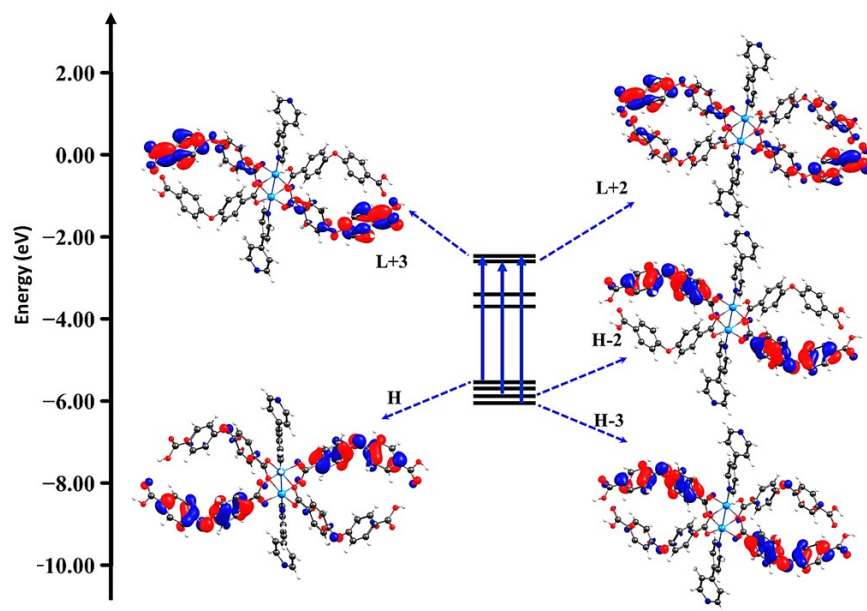

Figure 2. Molecular orbital energy diagram for Zn-MOF showing the vertical electronic transitions for the maxima absorption band at B3LYP/def2-TZVPP theoretical level.

In order to carry out a strong analysis of host-guest interactions, the Zn-MOF ground state was optimized with the incorporation of the analytes. The analytes were selected considering the reported largest and the lowest quenching efficiency of the Zn-MOF fluorescence; *i.e.* nitrobenzene (quenching, 84%) and toluene (non-quenching).[31] All Zn-MOF-analyte systems were optimized at the same theoretical level as the free Zn-MOF. The proposed input geometries consisted on the pi-staking/aromatic interaction between the linkers and target molecules. Two interaction models were considered for each analyte, one where the interaction occurs with the aromatic ring of the OBA linker while the other displays the interaction with the BPY fragment. Both initial structures converged to the host-guest interaction between the analyte and BPY, with a distance between them within the range of 3.15–3.34 Å. Zn-MOF-nitrobenzene and Zn-MOF-toluene minima structures were selected for the calculations and the analyzes described below. The geometrical parameters computed for the Zn-MOF interacting with the analytes did not show significant differences in relation to the ground state of the free Zn-MOF, see Table S1, Supporting Information.

Fluorescence Quenching Pathway

Frontier molecular orbital (FMO) analysis of host-guest systems showed that of electron density distribution changes upon the incorporation of an analyte with electron-acceptor ($-NO_2$) groups or electron-donor ($-CH_3$) groups, see Figure 3. The FMOs of Zn-MOF-toluene and Zn-MOF indicate that both systems exhibit similar features, as the HOMO in both systems exhibits that electron density is distributed on the OBA linkers while the LUMO is located on BPY linkers. In case of Zn-MOF-toluene, the molecular orbitals located on the guest molecule appear in a set of inner occupied molecular orbitals, as well as more external molecular orbital into the virtual space, see Figure S1 Supporting Information. However, when the guest is the NACs such as nitrobenzene, the HOMO is totally distributed on the OBA linkers whereas the LUMO is extended on the nitrobenzene framework, see Figure 3. These results are consistent with the reported by Ce Chao et al.[24] in regarding the analysis of the FMOs considering the interaction between Zn-MOF and analyte.
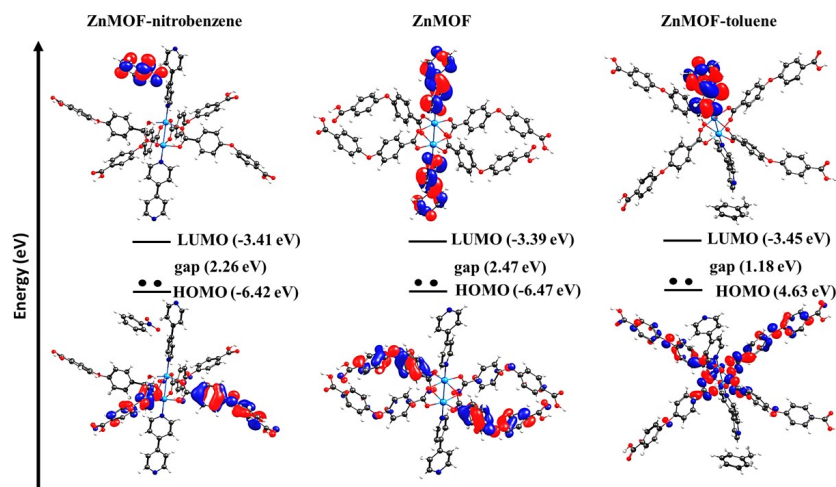
**Figure 3.** Frontier molecular orbitals of Zn-MOF and Zn-MOF-analyte systems.

Furthermore, TD-DFT calculations allowed us to confirm that the absorption spectra only implies electronic transitions involving active orbitals of the OBA linkers. This result was observed regardless of whether the systems do or do not have an analyte, see Table 2.

The absorption spectrum of the Zn-MOF-nitrobenzene showed that the molecular orbitals involved in the absorption bands are localized on the OBA linker. These molecular orbitals are presented in Figure 4, which evidences the excitations of intra-ligand charge-transfer (ILCT) character. Similar results were obtained for Zn-MOF-toluene computed at the same level of theory, see Figure S2 in the Supporting Information.

6

Table 2. Singlet - Singlet electronic transitions, absorption data, for Zn-MOF-analyte at B3LYP/ def2-TZVPP theoretical level.

Zn-MOF-analyte	λmax (nm)	f	Assignment	Active MO	Cts (%)
Zn-MOF-nitrobenzene	281	1.16	$\pi(\Lambda^{OBA})$-$\pi^*(\Lambda^{OBA})$	H-2-L+4	38
			$\pi(\Lambda^{OBA})$-$\pi^*(\Lambda^{OBA})$	H-L+6	18
			$\pi(\Lambda^{OBA})$-$\pi^*(\Lambda^{OBA})$	H-L+5	11
Zn-MOF-toluene	281	1.33	$\pi(\Lambda^{OBA})$-$\pi^*(\Lambda^{OBA})$	H-L+4	16
			$\pi(\Lambda^{OBA})$-$\pi^*(\Lambda^{OBA})$	H-L+5	12
			$\pi(\Lambda^{OBA})$-$\pi^*(\Lambda^{OBA})$	H-1-L+5	14

Where: H: is HOMO, L is LUMO, Cts (%) is contributions corresponding of electronic transitions
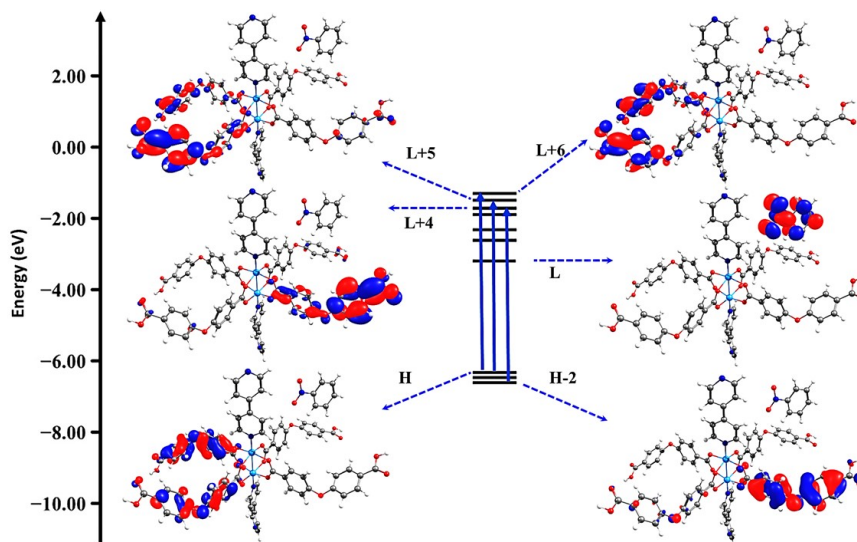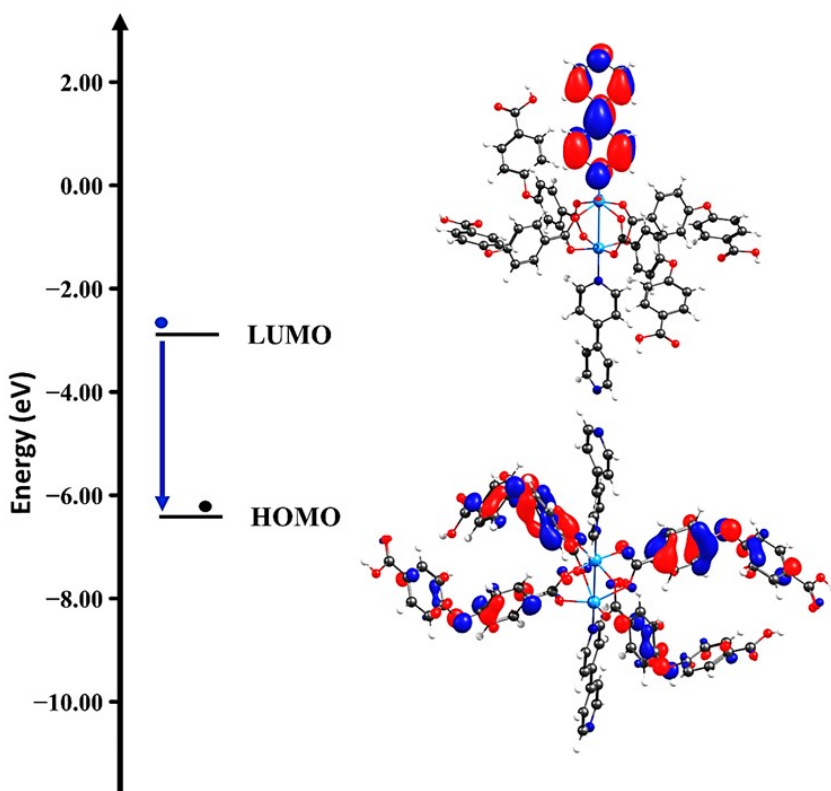

Figure 4. Molecular orbital energy diagram for Zn-MOF-nitrobenzene showing the vertical electronic transitions for the maxima absorption band at B3LYP/def2-TZVPP theoretical level.

The radiative deactivation of the excited state can occur by two mechanisms, fluorescence or phosphorescence, after photoexcitation. It is well-known since 1950, from Michael Kasha's works that "the emitting electronic level of a given multiplicity is the lowest excited level of that multiplicity" [49], which is known as the kasha's rule. In this sense, fluorescence is the emission processes, due to radiative deactivation from first excited singlet states to the ground state. In the particular case of phosphorescence, it is necessary to populate an excited triplet (T_1) with less energy than the first singlet excited S_1 state, this mechanism is known as an intersystem cross (ISC), for relaxes to its ground state.[50-51] The importance of the precise description of these states, the S_1 state or T_1 state, to understand the mechanisms by which activate or deactivate the luminescence in chemosensors optical has been emphasized by Briggs and Besley in 2015.[52] In recent studies,

our group proposed and verified a theoretical protocol, based on this statement, from the elucidation of the sensing mechanism in chemosensor selective to metal ions.

A precise description, both of the S_0 state and of the S_1 state, in terms of energy and structure, allowed us to explain in detail the turn-on fluorescent mechanism of the two chemosensor luminescent based in Schiff basis selective to metal ions.[53-54]

Considering the importance of knowing the emissive state of chemosensor is optimized S_1 state of the Zn-MOF to understand the origin of fluorescence in this system. Thus, the optimized geometry of the S_1 state was taken as input data to calculate the electronic transitions that constitute emission spectrum of Zn-MOF by means of TD-DFT methods. These calculations confirmed that the molecular orbitals involved in the emission band are linkers-localized. This result indicates that fluorescence is originated by a transition π-π* linker-centered from the LUMO to HOMO, whit 97% of contributions corresponding to this electronic transition. It also shows that the electron density of LUMO is located on the BYP linker, while the HOMO is localized on the OBA linkers see Figure 5. This result is consistent with those observed in other LMOFs based on metals ions d^{10} recently reported, which origin of emission is assigned to ligand-to-ligand charge transfer. [2212] This emission pathway is observed mainly in LMOFs based Zn^{2+} and Cd^{2+} since these ions with oxidation state $^{2+}$, tend to retain the d^{10} configuration.[5556]

Figure 5. Molecular orbital energy diagram for Zn-MOF-nitrobenzene showing the vertical electronic transitions for the maxima absorption band at B3LYP/def2-TZVPP theoretical level

Guang-Yue and Ke-Li in 2018 highlight that the host-guest interaction can be generated and that some molecular orbitals of guests appear located between the molecular orbitals involved in the emissive state, for that reason, radiative deactivation is blocked, resulting in the Turn-off .[57] In this sense, our results indicated that when nitrobenzene is confined into the Zn-MOF is generates a mixture of states of Zn-MOF

8

and nitrobenzene. In the Zn-MOF-nitrobenzene is observed that the analyte-centered molecular orbital corresponds to the LUMO, while the orbitals just above the LUMO are orbitals located on the BYP linker, which represent the molecular orbitals that correspond to the emissive states in analyte-free Zn-MOF, see Figure 6.
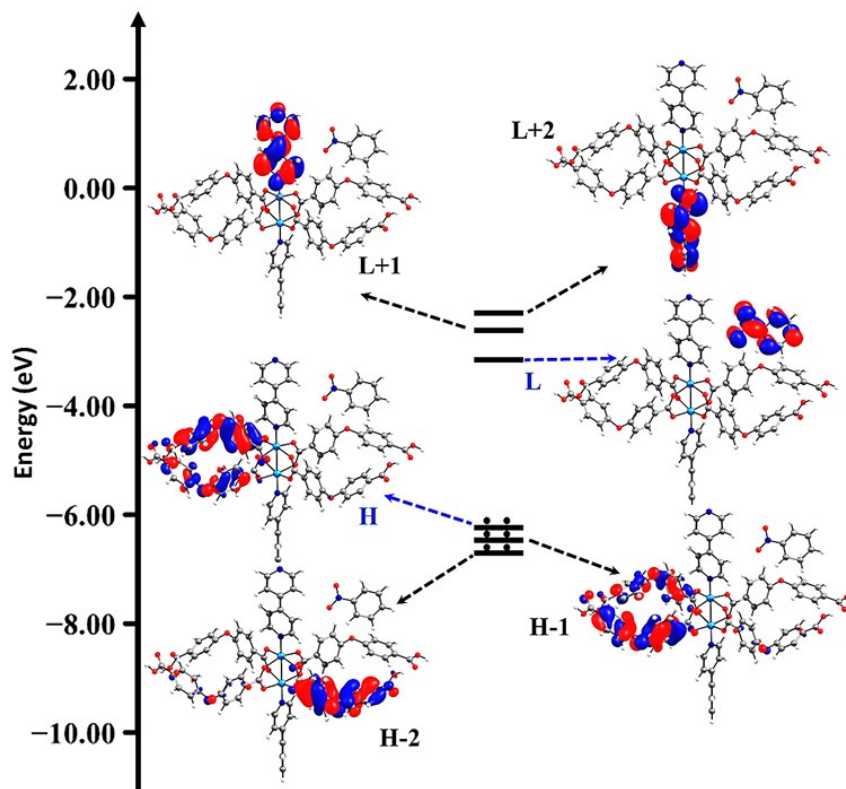
Figure 6. Frontier molecular orbitals of Zn-MOF-nitrobenzene.

Based on these results, the Franck-Condon principle and selection rules, we support the hypothesis that upon photoexcitation the electron relaxes until reaching the first excited electronic state, presumably located in de nitrobenzene, from which the dissipates of energy through the non-radiative transition. For that reason, the electron relaxation from PBY linker of the OBA linker is blocked resulting in the turn-off of the fluorescence. Besides, this electronic configuration of the coupled system Zn-MOF-nitrobenzene would explain the experimental interpretation of the quenching fluorescence is due to the LUMO of nitrobenzene appear below the emissive state of the MOF.[31]

Considering these results, this theoretical insight was carried out from another perspective based on a theoretical approach most commonly reported in the literature. This method consists of separately treating the electro-donor species, MOF, and electro-acceptor species, NACs, at the same level of theory. [58-59] The FMO analysis showed that the LUMO of the nitrobenzene is located lower energy level than the LUMO of Zn-MOF, see Figure 7, thus the photoinduced charge-transfer (PET) between Zn-MOF and nitrobenzene is possible.

9
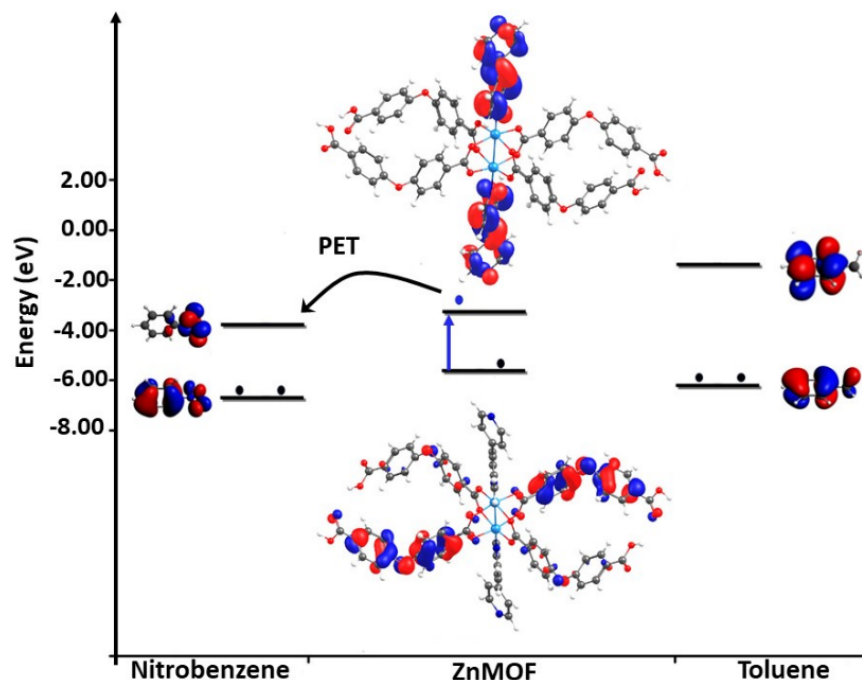
Figure 7. Calculated frontier molecular orbital energies (eV) of the nitrobenzene, toluene, and Zn-MOF.

These results are consistent with the quenching mechanism that has been widely accepted for this type of luminescence chemosensor for nitroaromatics compounds. According to literature, deactivation of the luminescent is produced by the transfer of electrons, after a photoinduced excitation, between the conduction band of MOF and lowest unoccupied molecular orbital of the analyte. [60-61]Finally, the calculations of Zn-MOF-toluene system showed that the active molecular orbitals are similar to the Zn-MOF without a guest. It should also be noted that according to observed experimentally, in the presence of toluene, it is not observed fluorescence attenuation. The result also suggests that the mixture of the Zn-MOF orbitals and the analyte orbitals in the active space has an important role in the quenching of fluorescence.

### Host-guest interaction based on Morokuma-Ziegler analysis

The analysis of host-guest interactions based on the Morokuma-Ziegler decomposition scheme has proven successful procedure for interpretation of the nature of the interaction between the two structures. In the case of MOFs, analysis of the interaction has recently been reported, considering the MOF and the guest as the two molecular fragments that constitute the whole system.[33-35]

From this perspective, the energy decomposition analyses (EDA) was carried out, where each system studied was divided into two fragments: Zn-MOF and the analyte (*i.e* . nitrobenzene and toluene). Due to our interest in the dispersive forces (van der Waals force) acting between the fragments [Zn-MOF] and [analyte], were incorporating Grimme's (D3) dispersion correction this analysis. According to the results, interaction energies for all systems does not exceed -6 kcal/mol, which indicates the predominant the long-range interactions. The Zn-MOF-analyte interactions are more intense in the case of analytes more electron-deficient (i.e. nitrobenzene), for which electrostatic interaction represents 51% of interaction energy. While the toluene, containing the electron-donating group, shows that weaker interaction energy with Zn-MOF, in which the dispersive contribution represents 67 %, see Table 3. These results evidence that in the case of the Zn-MOF-nitrobenzene is possible a charge transfer between the Zn-MOF and nitrobenzene.

Table 3. Morokuma–Ziegler's scheme energy decomposition analysis (EDA kcal/mol) of denoting the Zn-MOF-analyte interaction.

System	$\Delta E_{\Pi\alpha\upsilon\lambda\iota}$	$\Delta E_{E\lambda\epsilon\sigma\tau\alpha\tau}$	$\Delta E_{O\rho\beta}$	$\Delta E_{\Delta\iota\sigma\pi}$	$\Delta E_{\Delta\iota\sigma\pi}$	$\Delta E_{I\nu\tau}$
Zn-MOF-nitrobenzene	2.35	-3.76 (51%)	-1.13(15%)	-2.53(34%)	-2.53(34%)	-5.60
Zn-MOF-toluene	0.89	-0.86 (23%)	-0.36 (10%)	-2.52 (67%)	-1.07	-1.07

In this context, an analysis via the NOCV approach can provide useful information on the channels of charge transfer between the fragments. While it is true that both systems the interaction energy have weak the covalent character, the NOCV analysis revealed that the interaction host-guest involves a charge transfer or donor-acceptor interactions. As observed in Figure 8, the plots of NOCV deformation density (ρ) for Zn-MOF-analyte systems are can be identified of the deformation density channel between the host and guest. These charge density accumulations describe intermolecular interaction, between the BPY linker of Zn-MOF and analyte. Taking into account that the coupled Zn-MOF-nitrobenzene system, generates that the orbitals localized on the BPY linkers appear just above the LUMO orbital (totally located on the of nitrobenzene), it may be possible to occur intermolecular PET from Zn-MOF to nitrobenzene.
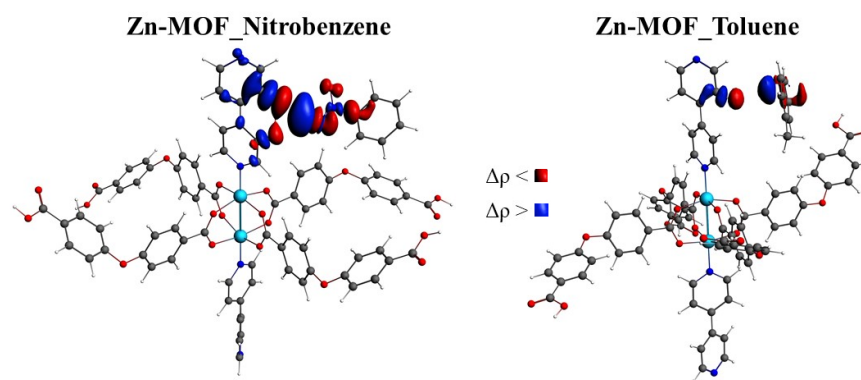
Figure 8 . NOCV-based deformation densities ($\Delta\rho$) for the host-guest interactions for Zn-MOF-analytes.

Conclusions

Quantum chemical approaches were successfully employed to assess the relationship between the structure of the LMOF and analyte-induced luminescence change.

First, we found that the molecular orbitals involved in the absorption bands of the spectrum profile of the Zn-MOF, are localized on the 4,4'-oxybis (benzoic acid) (OBA) linker. Besides, the emission phenomenon was characterized as fluorescence emission *via* LLCT processes, which takes place from 4,4'-bipyridine (BYP) to the 4,4'-oxybis (benzoic acid) (OBA) linker. As second part of the work, analyte (nitrobenzene) confinement was studied into the Zn-MOF, which gave rise to a mixture of the molecular orbitals from both systems. Interesting, the LUMO corresponds to orbitals of the nitrobenzene and appears energetically close to the molecular orbital localized at the BYP, which is involved in the emissive state of the free Zn-MOF. These results suggest that the LUMO, located on nitrobenzene, blocked the LLCT process between BPY and OBA, leading to the fluorescence quenching. Therefore, it is demonstrated that the simulation of the host-guest system is imperative to understand the luminescence changes that govern the sensing mechanism in a chemosensor. Otherwise, the study of the interaction via the Morokuma-Ziegler decomposition scheme and Natural Orbital of Chemical Valence (NOCV) analysis, proposed by the Mitoraj, were useful to propose possible channels of charge transfer between Zn-MOF and nitrobenzene.

In summary, the intention of this study was to get theoretical insights into the sensing mechanism MOF chemosensor selective to nitrobenzene through analysis of host-guest interactions. Due to the large size of

this system, it was applied a fragmentation scheme of experimental X-ray single-crystal data of the Zn-MOF, reaching a finite structural model $[Zn_2(OBA)_4(BYP)_2]$ to optimize time and computational resources. This structural model has satisfactorily reproduced geometry parameters and photophysical properties of the Zn-MOF with and without the analyte.

Funding Information

References

1. Y. Deng, N. Chen, Q. Li, X. Wu, X. Huang, Z. Lin and Y. Zhao, *Cryst. Growth Des.* , **2017** , 17, 3170–3177.

2. T. K. Kim, J. H. Lee, D. Moon and H. R. Moon, *Inorg. Chem.* , **2013** , 52, 589–595.

3. F. M. Wang, L. Zhou, W. P. Lustig, Z. Hu, J. F. Li, B. X. Hu, L. Z. Chen and J. Li, *Cryst. Growth Des.* , **2018** , 18, 5166–5173.

4. A. Karmakar, P. Samanta, A. V. Desai and S. K. Ghosh, *Acc. Chem. Res.* , **2017** , 50, 2457–2469.

5. S. S. Nagarkar, B. Joarder, A. K. Chaudhari, S. Mukherjee and S. K. Ghosh, *Angew. Chemie - Int. Ed.* , **2013** , 52, 2881–2885.

6. E. V. Verbitskiy, A. A. Baranova, K. I. Lugovik, M. Z. Shafikov, K. O. Khokhlov, E. M. Cheprakova, G. L. Rusinov, O. N. Chupakhin and V. N. Charushin, *Anal. Bioanal. Chem.* , **2016** , 408, 4093–4101.

7. B. Gole, A. K. Bar and P. S. Mukherjee, *Chem. - A Eur. J.* , **2014** , 20, 2276–2291.

8. F. Wang, Z. Yu, C. Wang, K. Xu, J. Yu, J. Zhang, Y. Fu, X. Li and Y. Zhao, *Sensors Actuators, B Chem.* , **2017** , 239, 688–695.

9. Y. Zhang, S. Yuan, G. Day, X. Wang, X. Yang and H. C. Zhou, *Coord. Chem. Rev.* , **2018** , 354, 28–45.

10. Y. Liu, A. J. Howarth, N. A. Vermeulen, S. Moon, J. T. Hupp and O. K. Farha, *Coord. Chem. Rev.* , **2017** , 346, 101–111.

11. W. P. Lustig, S. Mukherjee, N. D. Rudd, A. V. Desai, J. Li and S. K. Ghosh, *Chem. Soc. Rev.* , **2017** , 46, 3242–3285.

12. Z. Hu, B. J. Deibert and J. Li, *Chem. Soc. Rev.* , **2014** , 43, 5815–5840.

13. B. Karadeniz, A. J. Howarth, T. Stolar, T. Islamoglu, I. Dejanović, M. Tireli, M. C. Wasson, S. Y. Moon, O. K. Farha, T. Friščić and K. Užarević, *ACS Sustain. Chem. Eng.* , **2018** , 6, 15841–15849.

14. M. Rimoldi, A. J. Howarth, M. R. Destefano, L. Lin, S. Goswami, P. Li, J. T. Hupp and O. K. Farha, *ACS Catal.* , **2017** , 7, 997–1014.

15. Y. Cui, Y. Yue, G. Qian and B. Chen, *Chem. Rev.* , **2012** , 112, 1126–1162.

16. S. S. Nagarkar, A. V. Desai and S. K. Ghosh, *Chem. Commun.* , **2014** , 50, 8915–8918.

17. K. J. Kim, P. Lu, J. T. Culp and P. R. Ohodnicki, *ACS Sensors* , **2018** , 3, 386–394.

18. Y. Cui, J. Zhang, B. Chen and G. Qian, *Lanthanide Metal-Organic Frameworks for Luminescent Applications* , Elsevier B.V., 1st edn., **2016** , vol. 50.

19. H. S. Jung, K. C. Ko, J. H. Lee, S. H. Kim, S. Bhuniya, J. Y. Lee, Y. Kim, S. J. Kim and J. S. Kim, *Inorg. Chem.* , **2010** , 49, 8552–8557.

20. E. A. Dolgopolova, A. M. Rice, C. R. Martin and N. B. Shustova, *Chem. Soc. Rev.* , **2018** , 47, 4710–4728.

21. C. A. Bauer, T. V. Timofeeva, T. B. Settersten, B. D. Patterson, V. H. Liu, B. A. Simmons and M. D. Allendorf, *J. Am. Chem. Soc.* , **2007** , 129, 7136–7144.

22. L. Lu, W. Liu, J. Wang, H. Zhong, J. Liu, A. K. Singh and A. Kumar, *Inorganica Chim. Acta* , **2019** , 487, 257–263.

23. W. P. Lustig, F. Wang, S. J. Teat, Z. Hu, Q. Gong and J. Li, *Inorg. Chem.* , **2016** , 55, 7250–7256.

24. P. Wang, X. Song, Z. Zhao, L. Liu, W. Mu and C. Hao, *Chem. Phys. Lett.* , **2016** , 661, 257–262.

25. B. Gole, A. K. Bar and P. S. Mukherjee, *Chem. - A Eur. J.* , **2014** , 20, 13321–13336.

26. M. Raizada, F. Sama, M. Ashafaq, M. Shahid, M. Khalid, M. Ahmad and Z. A. Siddiqi, *Polyhedron* , **2018** , 139, 131–141.

27. G. Settanni, J. Zhou, T. Suo, S. Schöttler, K. Landfester, F. Schmid and V. Mailänder, *Chem. Soc. Rev. Manuscr.* , **2015** , 44, 8019–8061.

28. B. Joarder, A. V. Desai, P. Samanta, S. Mukherjee and S. K. Ghosh, *Chem. - A Eur. J.* , **2015** , 21, 965–969.

29. T. K. Kim, J. H. Lee, D. Moon and H. R. Moon, *Inorg. Chem.* , **2013** , 52, 589–595.

30. K. Müller-Buschbaum, F. Beuerle and C. Feldmann, *Microporous Mesoporous Mater.* , **2015** , 216, 171–199.

31. S. Pramanik, C. Zheng, X. Zhang, T. J. Emge and J. Li, *J. Am. Chem. Soc.* , **2011** , 133, 4153–4155.

32. T. Ziegler and A. Rauk, *Theor. Chim. Acta* , **1977** , 46, 1–10.

33. R. Guajardo-Maturana, X. Zarate, F. Claveria-Cadiz and E. Schott, *RSC Adv.* , **2016** , 6, 103346–103356.

34. S.-R. Zhang, D.-Y. Du, J.-S. Qin, S.-J. Bao, S.-L. Li, W.-W. He, Y.-Q. Lan, P. Shen and Z.-M. Su, *Chem. - A Eur. J.* , **2014** , 20, 3589–3594.

35. J. Poater, M. Gimferrer and A. Poater, *Inorg. Chem.* , **2018** , 57, 6981–6990.

36. J. Q. and C. H. Lei Liu, Xiaofang Chen, *Dalt. Trans.* , **2015** , 44(6), 2897–2906.

37. I. Weinrauch, I. Savchenko, D. Denysenko, S. M. Souliou, H. H. Kim, M. Le Tacon, L. L. Daemen, Y. Cheng, A. Mavrandonakis, A. J. Ramirez-Cuesta, D. Volkmer, G. Schütz, M. Hirscher and T. Heine, *Nat. Commun.* , **2017** , 8, 1–7.

38. V. Bernales, M. A. Ortuño, D. G. Truhlar, C. J. Cramer and L. Gagliardi, *ACS Cent. Sci.* , **2018** , 4, 5–19.

39. D. Peled, V. Pratt and G. Holzmann, *Chem. Commun.* , **2014** , 50, 8944–8946.

40. F. Neese, *Comput. Mol Sci* , **2012** , 2, 73–78.

41. J. P. Perdew and W. Yue, *Phys. Rev. B* , **1986** , 33, 8800–8802.

42. F. Weigend and R. Ahlrichs, *Phys. Chem. Chem. Phys.* , **2005** , 7, 3297–3305.

43. A. D. Becke, *J. Chem. Phys.* , **1993** , 98, 1372–1377.

44. T. Yanai, D. P. Tew and N. C. Handy, *Chem. Phys. Lett.* , **2004** , 393, 51–57.

45. K. Kitaura and K. Morokuma, *Int. J. Quantum Chem.* , **1976** , 10, 325–340.

46. M. P. Mitoraj, *J Mol Model* , **2013** , 19, 4681–4688.

47. M. P. Mitoraj, *J. Phys. Chem. A* , **2011** , 115, 14708–14716.

48. S. Grimme, J. Antony, S. Ehrlich and H. Krieg, *J. Chem. Phys.* , **2010** , 132.

49. B. Y. M. Kasha, *Discuss. Faraday Soc.* , **1950** , 9, 14–19.

50. J. Heine and K. Müller-Buschbaum, *Chem. Soc. Rev.* ,**2013** , 42, 9232.

51. H. W. Tseng, J. Y. Shen, T. Y. Kuo, T. S. Tu, Y. A. Chen, A. P. Demchenko and P. T. Chou, *Chem. Sci.* , **2016** , 7, 655–665.

52. E. a. Briggs and N. a. Besley, *J. Phys. Chem. A* ,**2015** , 119, 2902–2907.

53. M. A. Treto-Suárez, Y. Hidalgo-Rosa, E. Schott, X. Zarate and D. Páez-Hernández, *J. Phys. Chem. A* , **2019** , 123, 6970–6977.

54. M. A. Treto-Suárez, Y. Hidalgo-Rosa, E. Schott, X. Zarate and D. Páez-Hernández, *Int. J. Quantum Chem.* , **2019** , 1–10.

55. L. Wen, D. Dang, C. Duan, Y. Li, Z. Tian and Q. Meng, *Inorg. Chem.* , **2005** , 44, 7161–7170.

56. W. Liu, L. Ye, X. Liu, L. Yuan, J. Jiang and C. Yan,*CrystEngComm* , **2008** , 10, 1395.

57. G. Y. Li and K. L. Han, *Wiley Interdiscip. Rev. Comput. Mol. Sci.* , **2018** , 8, 1–17.

58. Z. Hu, B. J. Deibert and J. Li, *Chem. Soc. Rev.* ,**2014** , 43, 5815–5840.

59. X.-J. Zhang, F.-Z. Su, D.-M. Chen, Y. Peng, W.-Y. Guo, C.-S. Liu and M. Du, *Dalt. Trans.* , **2019** .

60. L. Zhang, Z. Kang, X. Xin and D. Sun, *CrystEngComm* ,**2016** , 18, 193–206.

61. W. P. Lustig, S. Mukherjee, N. D. Rudd, A. V. Desai, J. Li and S. K. Ghosh, *Chem. Soc. Rev.* , **2017** , 46, 3242–3285.